$BiMO_x$ Semiconductor as Catalysts for Photocatalytic Decomposition of N_2O: A Combination of Experimental and DFT+U Study

Jixing Liu,[†,§] Lu Wang,[†,§] Weiyu Song,[†,§] Minjie Zhao,[†] Jian Liu,*[,†] Hong Wang,[‡] Zhen Zhao,[†] Chunming Xu,[†] and Zhichen Duan[†]

[†] State Key Laboratory of Heavy Oil and Beijing Key Lab of Oil & Gas Pollution Control, China University of Petroleum, Beijing 102249, P. R. China;

[‡] College of Chemical Engineering, Beijing Institute of Petrochemical Technology/Beijing Key Laboratory of Fuels Cleaning and Advanced Catalytic Emission Reduction Technology, Beijing 102617, China;

* Corresponding author: E-mail address: liujian@cup.edu.cn

[1] Postal Address: 18# Fuxue Road, Chang Ping District, Beijing, 102249, China,

Tel: 86-10-89732278, Fax: 86-10-69724721;

[2] Postal Address: 19# Qingyuan North Road, Da Xing District, Beijing, 102617, China,

Tel: 86-10-81292131;

The supporting information contains 15 pages, 1 table and 8 pictures

Activity Evaluation

Schematics of experimental device of N_2O photocatalytic decomposition was exhibited in Figure S1.

Characterization of Catalyst

The structure and crystal phases of the as-prepared photocatalysts were determined by X-ray diffractometer (XRD) patterns with 2θ ranges from 5−80 °. The equipment is Shimadzu XRD-7000 diffractometer with Cu Ka radiation (k = 1.5406 Å) and performed at 40 kV and 30 mA.

Specific surface area was determined using a Quadrasor SI instrument (Micromeritics Instruments, USA) after degassing of materials at 300 ℃ for 3 h to remove physisorbed water. The measured data were processed according to the BET isotherm within the range of P/P_o = 0−1 at 77 K.

The Raman spectra were obtained with a 10 mW Ar^+ laser (532 nm) and a 50× long-focus lens. The time and power of acquisition were 10 s and 5%.

The morphology of the samples was characterized by a field emission scanning electron microscopy (SEM, FEI Quanta 200F). Before the SEM analysis, the samples were sputtered by gold (Polaron Range SC 7640) in the argon atmosphere.

Transmission electron microscopy (TEM) images were taken on a Tecnai G2 F20 electron micro-scope operated at 200 kV. The catalysts were suspended in ethanol and dispersed over a carbon-coated holey Cu grid with a film prior to measurements.

X-ray photoelectron spectroscopy (XPS) spectra were collected on an ESCALAB 250 spectrometer equipped with Al K_α (150 W) radiation. The binding energies were calibrated using C1s peak of contaminant carbon (BE = 284.8 eV) as an internal standard. Deconvolution of Bi 2p, V 3d, Mo 3d, W 3d and O 1s peak of catalysts was performed on origin 8.5 software.

Diffuse reflectance (DR) UV-vis spectra of the products were recorded on a Shimadzu UV-4100 spectrophotometer with $BaSO_4$ as reflectance standard.

The photoluminescence (PL) spectra were conducted on an F-7000 spectrophotometer with

excitation wavelength of 400 nm. The signal of carbon at 284.8 eV was used as a reference to calibrate the binding energy.

Electrochemical characters of materials were performed on a CHI-660E electrochemical workstation using a platinum electrode as the counter electrode, and a saturated calomel electrode as the reference electrode in a standard three electrode cell, respectively. The electrolyte was 0.2 mol/L Na_2SO_4 aqueous solution. The working electrode was prepared by dispersing amount of as-prepared material in 1 mL dimethylformamide and then spreading it on a cleaned fluoride-tin oxide (FTO) glass electrode (1.5 cm × 1.0 cm). Finally, the electrodes were calcined at 200 ℃ for 2 h. The electrochemical impedance measurements were conducted via a two probe method. All experiments were carried out with oscillation amplitude of 50 mV and frequency range between 100 Hz and 100 KHz.

Computational Details

All calculations were conducted using density functional theory (DFT) within the plane-wave pseudopotential as implemented in the VASP code with a cutoff energy of 500 eV. The Perdew, Burke, and Ernzerhof (PBE) exchange-correlation functional within a generalized gradient approximation (GGA) were employed.[1] The PAW method was used to describe the effect of core electrons.[2,3] A (2 × 2 × 1) k-point mesh was used for all geometry optimization, and a (9 × 9 × 1) mesh was utilized for electronic structure calculation. The atomic positions were relaxed until the force on each atom was less than 0.05 eV/Å. Using the periodic slab model and self-consistent dipole correction, the averaging electrostatic potential in the planes perpendicular to the slab normal could be obtained.

The optical absorption properties (as shown in Figure S4) of $BiVO_4$, Bi_2MoO_6, and Bi_2WO_6 were evaluated by absorption coefficient α(ω) defined as Equation S1:[9]

$$I(\omega) = \sqrt{2}\omega\left[\sqrt{\varepsilon_1^2(\omega)+\varepsilon_2^2(\omega)}-\varepsilon_1(\omega)\right]^{\frac{1}{2}} \quad \text{(S1)}$$

Where, ω is light frequency, $\varepsilon_1(\omega)$ and $\varepsilon_2(\omega)$ are real part and imaginary part in the dielectric

function, respectively. The real part $\varepsilon_1(\omega)$ of the dielectric function is evaluated from the imaginary part $\varepsilon_2(\omega)$ by Kramer-Kronig trans-formation. The imaginary part of the dielectric function can be given by the following Equation S2:[10]

$$\varepsilon_2(\hbar\omega) = \frac{2\ell^2\pi}{\Omega\varepsilon_0}\sum\kappa,\nu,\mathrm{c}\left|\langle\psi_\kappa^{\mathrm{c}}|\mu\gamma|\psi_\kappa^{\nu}\rangle\right|^2\delta(\mathrm{E}_\kappa^{\mathrm{c}}-\mathrm{E}_\kappa^{\nu}-\mathrm{E}) \quad \text{(S2)}$$

Where, Ω, ω, u, v, and c are unit-cell volume, photon frequencies, vector defining the polarization of the incident electric field, valence band states, and conduction band states, respectively.

To reduce the error of polar surfaces, dipole correction was considered. We used DFT+U method to minimize the error of DFT calculations for materials containing V (U = 4), Mo (U = 3) and W (U = 6).[4–6] To simulate a photogenerated electron, one electron was added.[7,8] In calculation section, to investigate the reaction, a hydrogen atom is introduced on the surface O atom to become a proton with an apparent charge state of +1. The electron from this H atom redistributes over V, Mo, and W atoms to populate the bottom of the $BiVO_4$, Bi_2MoO_6, and Bi_2WO_6 CB (Conduction Band), respectively. This electron mimics a photoexcited electron in these reactionsThe bulk equilibrium lattice constant of $BiVO_4$ is: a = b = 5.14 Å, c = 11.72 Å. The bulk equilibrium lattice constant of Bi_2MoO_6 is: a = 5.49 Å, b = 16.23 Å, c = 5.51 Å, and the bulk equilibrium lattice constant of Bi_2WO_6 is: a = 5.46 Å, b = 5.43 Å, c = 16.43 Å. The models of $BiMO_x$ are shown in Figure S5. We built a periodic slab with four, three and three layers for $BiVO_4$, Bi_2MoO_6, and Bi_2WO_6 surfaces, respectively. 2×2 surface unit cells were used, respectively. The bottom layer of $BiMO_x$ is fixed, while the top two layers are relaxed during the calculation. The vacuum gap thickness is set to be 12 Å.

Supplementary computational details of the relative level of CBM (Conduction Band Minimum) for $BiVO_4$ (011) and (111) surface.

We calculated the local potential of $BiVO_4$ along the z-axis of (011) surface and (113) surface, which are displayed in Figure S6A and S6B. We selected a point deep in the vacuum (16 Å) as the reference energy for (011) surface and (113) surface. In this point, the local potential is 4.19 and 5.06 eV, respectively. The difference of electrostatic potential is -0.87 eV. The original CBM for (011) surface and (113) surface are 1.02 and 0.63 eV, respectively. Therefore, the CBM for $BiVO_4$ (011) surface is 1.26 eV, which is higher than that for (113) surface, and the CBM for (011) surface is 1.26 eV that is higher than that for (113) surface.

For the same calculation method, in the point (16 Å), the local potential of Bi_2MoO_6 (002) and (112) surface are 3.22 and 5.58 eV, respectively (Figure S7). The original CBM for (002) surface and (112) surface are -0.03 and 0.64 eV, respectively. The CBM for Bi_2MoO_6 (002) surface is 1.69 eV higher than that for (112) surface. In the point (20 Å), the local potential of Bi_2WO_6 (200) and (131) surface are 4.37 and 4.60 eV, respectively (Figure S8). The original CBM for (200) surface and (131) surface are −0.06 and 0.04 eV, respectively. The CBM for Bi_2WO_6 (200) surface is 0.15 eV, which is higher than that for (131) surface.

Table S1 The Ratio of the Integral Area and the Conduction Band of M (V, Mo, W).

catalyst	integral area of M conduction band	integral area of $BiMO_x$ conduction band	ratio
$BiVO_4$	13.60	40.00	25.8%
Bi_2MoO_6	10.33	28.00	48.6%
Bi_2WO_6	10.43	40.00	26.1%

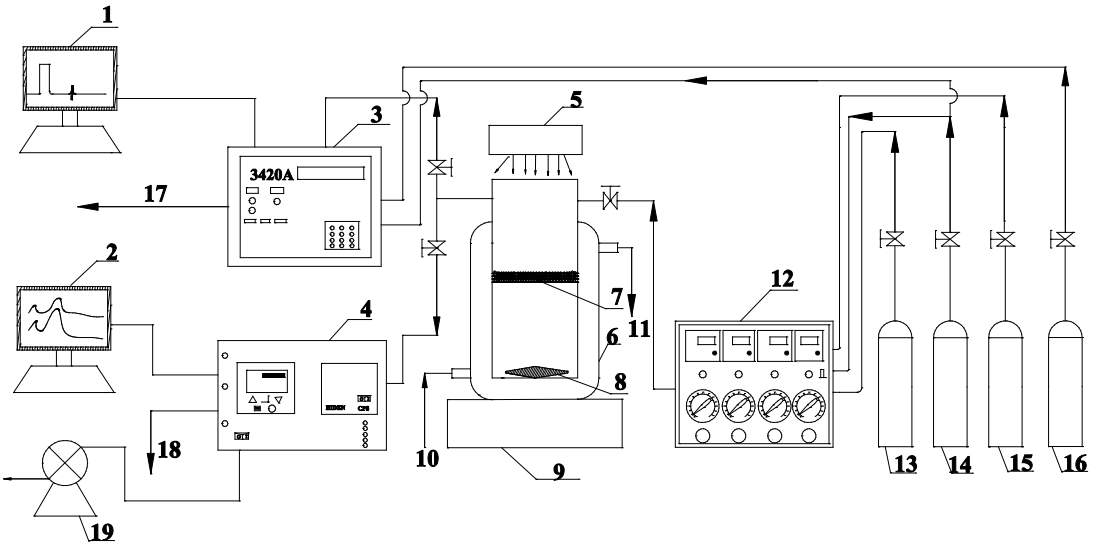

Figure S1 Schematics of experimental device of N_2O photocatalytic decomposition: 1. Chromatographic workstation; 2. Mass spectrometer work station; 3. Gas chromatograph; 4. Mass spectrograph; 5. Illuminant; 6: Photocatalytic reaction apparatus; 7. Catalyst; 8. Magnet rotor; 9. Magnetic stirrers; 10. Circulation water inlet valve; 11. Circulating water outlet valve; 12. Gas supply system; 13. O_2/Ar; 14. Ar; 15. N_2O/Ar; 16. H_2; 17. Venting; 18. Venting; 19. Bypass pump.

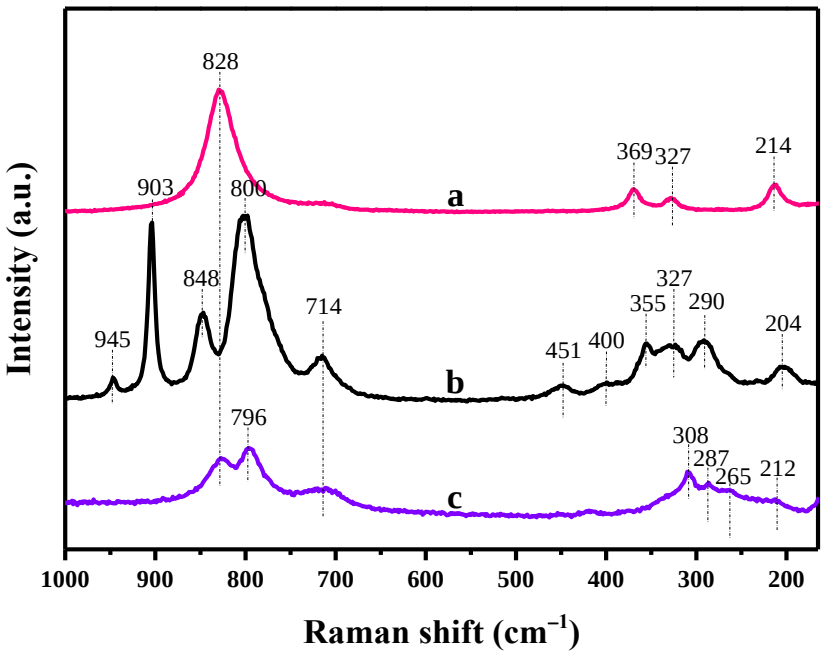

Figure S2 Raman spectra of the photocatalysts: (a) $BiVO_4$; (b) Bi_2MoO_6; and (c) Bi_2WO_6.

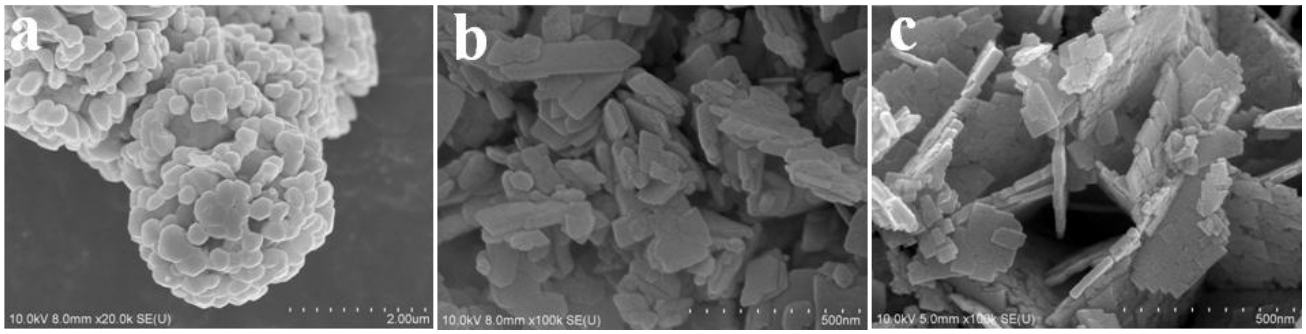

Figure S3 SEM images of the photocatalysts: (a) $BiVO_4$; (b) Bi_2MoO_6; and (c) Bi_2WO_6.

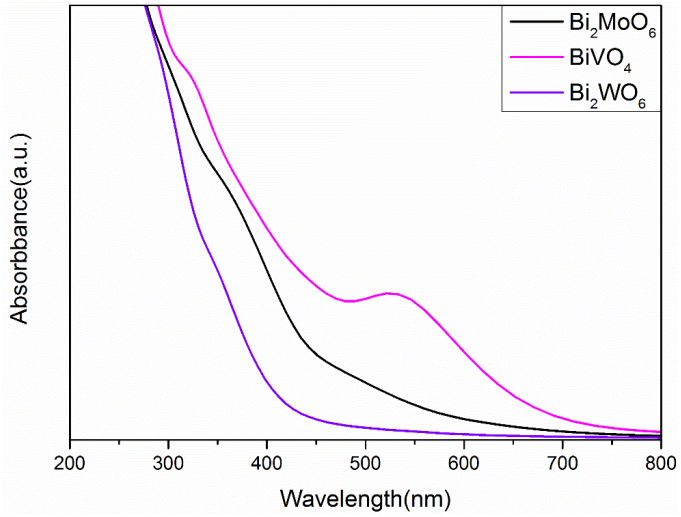

Figure S4 Optical absorption spectra of $BiVO_4$; Bi_2MoO_6; and Bi_2WO_6.

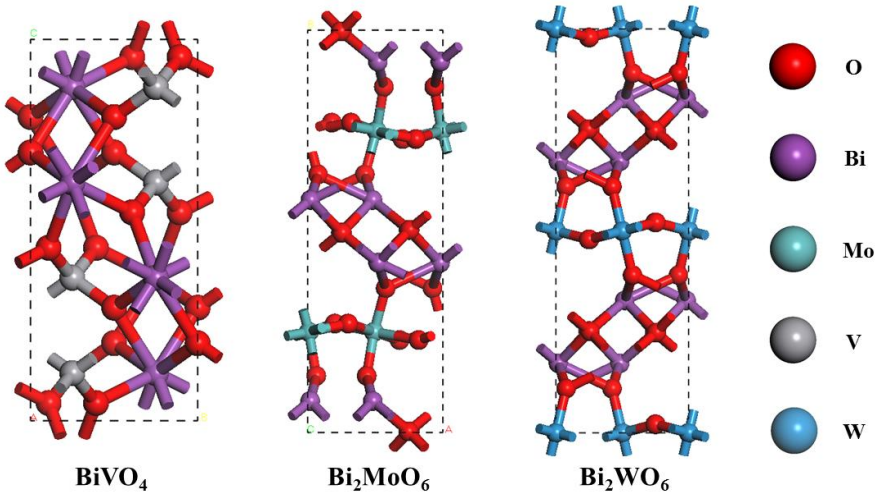

Figure S5 The crystallographic models of $BiVO_4$; Bi_2MoO_6; and Bi_2WO_6.

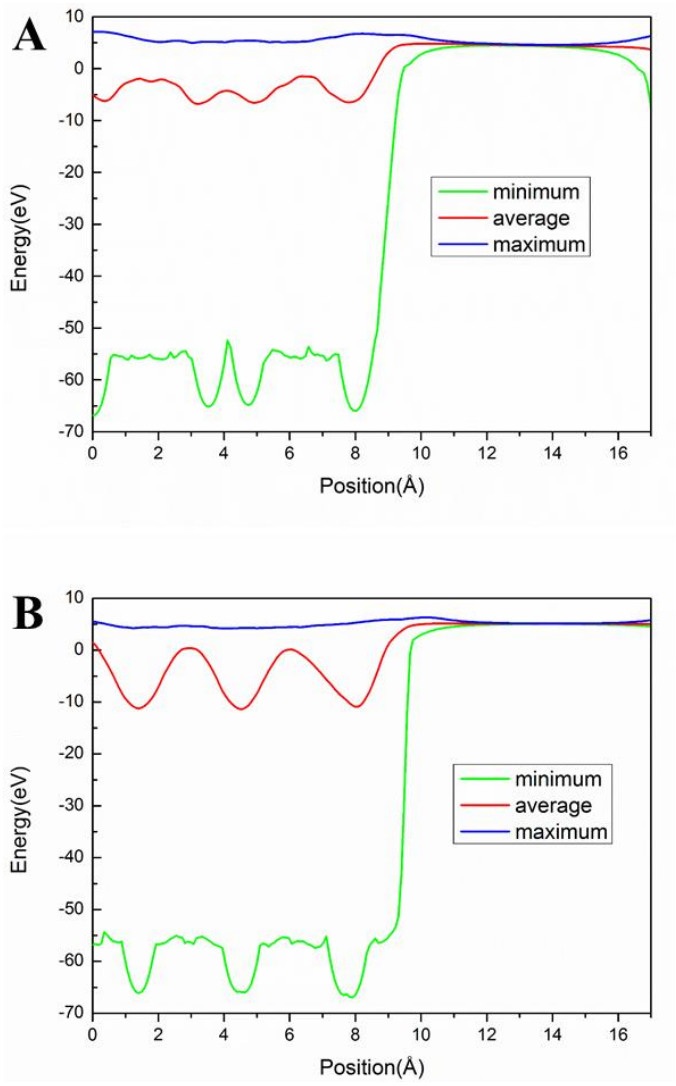

Figure S6 The local potential along the z-axis of the $BiVO_4$ surface: (A) (011) surface; and (B) (113) surface

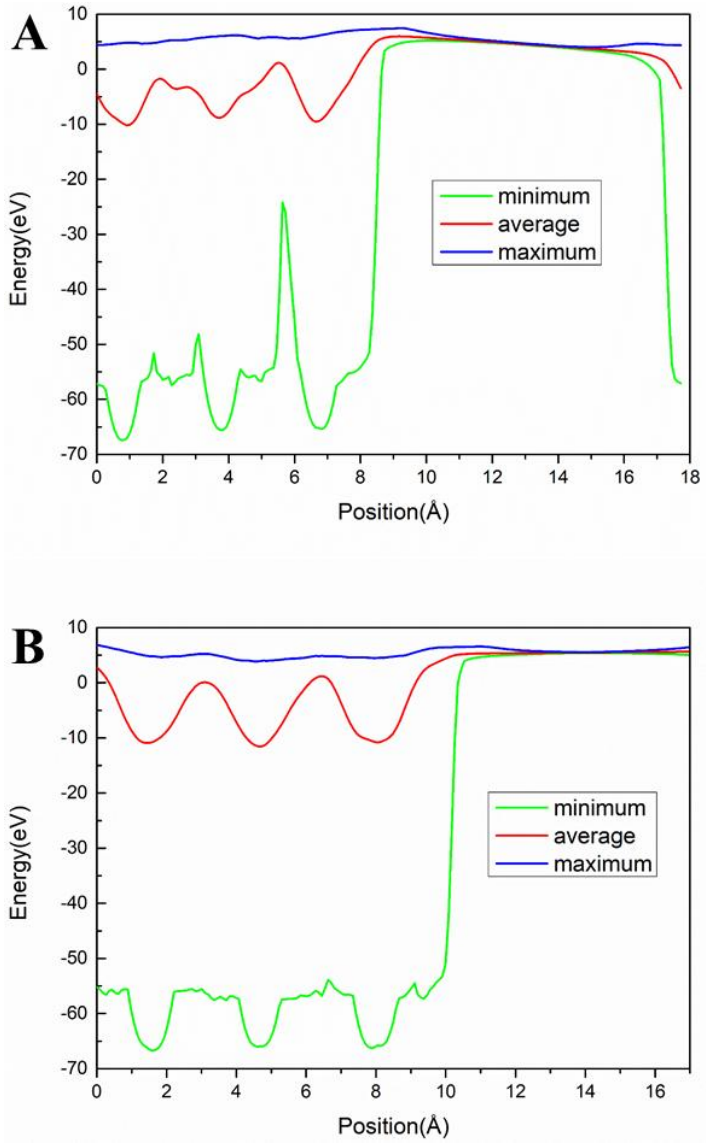

Figure S7 The local potential along the z-axis of the Bi_2MoO_6 surface: (A) (002) surface; and (B) (112) surface

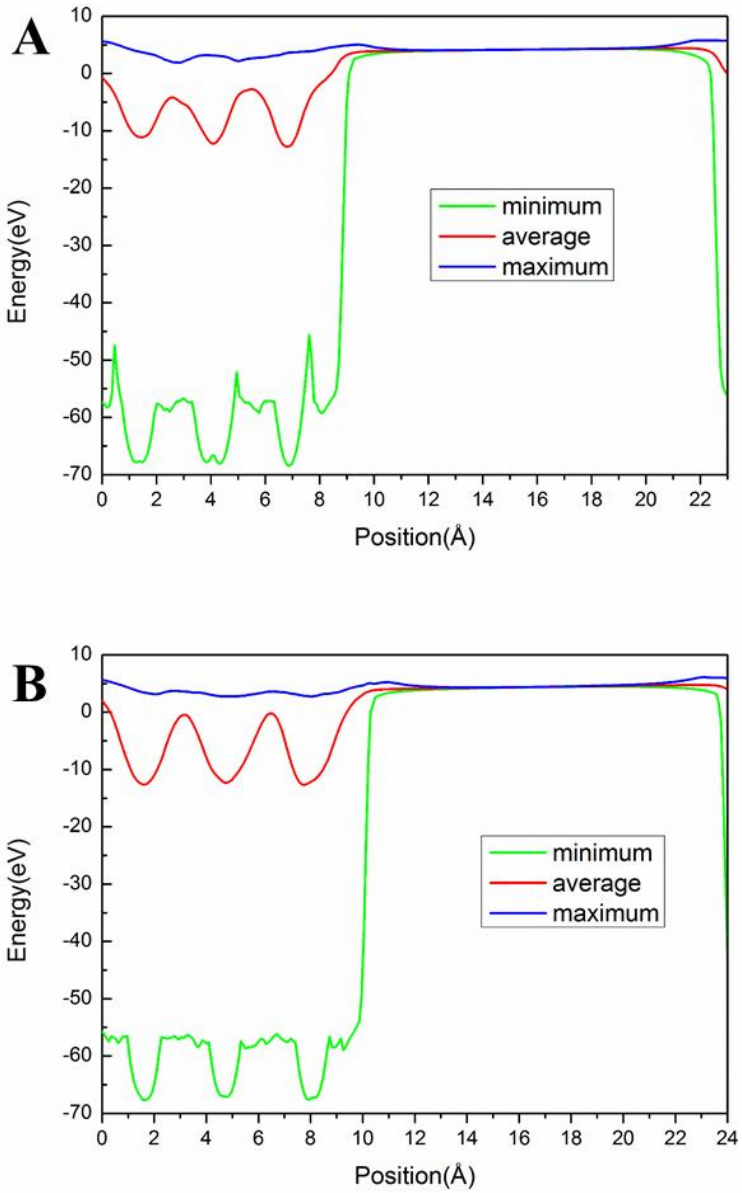

Figure S8 The local potential along the z-axis of the Bi_2WO_6 surface: (A) (200) surface; and (B) (131) surface

Literature Cited

(1) Perdew, J. P.; Burke, K.; Ernzerhof, M. Generalized gradient approximation made simple. *Phys. Rev. Lett.* **1996**, *77*, 3865−3868.

(2) Blöchl, P. E. Projector augmented-wave method. *Phys. Rev. B* **1994**, *50*, 17953−17979.

(3) Kresse, G.; Joubert, D. From ultrasoft pseudopotentials to the projector augmented-wave method. *Phys. Rev. B* **1999**, *59*, 1758−1775.

(4) Solovyev, I.; Hamada, N.; Terakura, K. t2g versus all 3d localization in $LaMO_3$ perovskites (M = Ti-Cu): First-principles study. *Phys. Rev. B* **1996**, *53*, 7158-7170.

(5) Baldoni, M.; Craco, L.; Seifert, G, Leoni, S. A two-electron mechanism of lithium insertion into layered α-MoO_3: A DFT and DFT+ U study. *J. Mater. Chem. A* **2013**, *1*, 1778-1784.

(6) Bondarenko, N.; Eriksson, O.; Skorodumova, N. V. Polaron mobility in oxygen-deficient and lithium-doped tungsten trioxide. *Phys. Rev. B* **2015**, *92*, 165119.

(7) Liu, D.; Li, L.; Gao, Y.; Wang, C.; Jiang, J.; Xiong, Y. The nature of photocatalytic "water splitting" on silicon nanowires. *Angew. Chem. Int. Ed.* **2015**, *54*, 1-7.

(8) Deskins, N. A.; Dupuis, M. Intrinsic hole migration rates in TiO_2 from density functional theory. *J. Phys. Chem. C* **2008**, *113*, 346-358.

(9) Read, A. J.; Needs R. J. Calculation of optical matrix elements with nonlocal pseudopotentials. *Phys. Rev. B: Condens. Matter Mater. Phys.* **1991**, *44*, 13071.

(10) Saha, S.; Sinha, T. P.; Mookerjee, A. Electronic structure, chemical bonding, and optical properties of paraelectric $BaTiO_3$. *Phys. Rev. B: Condens. Matter Mater. Phys.* **2000**, *62*, 8828.